Baghdad Science Journal

Volume 23 | Issue 1 Article 8

1-1-2026

Hematite/NiO/Graphene Composites: Enhancing Humidity Energy Harvesting Through Temperature Variations

Nurul Syafiqah Mohamed Mustakim
NANO-ElecTronic Centre (NET), Faculty of Electrical Engineering, Universiti Teknologi MARA, 40450 Shah Alam, Selangor, Malaysia, nurulsyafiqah273@gmail.com

Dayana Kamaruzaman
Faculty of Electrical Engineering, Universiti Teknologi MARA Cawangan Terengganu, Kampus Dungun, 23000 Dungun, Terengganu, Malaysia, dayana620@uitm.edu.my

Norfarariyanti Parimon
Faculty of Engineering, Universiti Malaysia Sabah, 88400 Kota Kinabalu, Sabah, Malaysia, fara2012@ums.edu.my

Mohd Khairul Ahmad
Microelectronic and Nanotechnology–Shamsuddin Research Centre (MiNT-SRC), Faculty of Electrical and Electronic Engineering, Universiti Tun Hussein Onn Malaysia, Batu Pahat Johor, Parit Raja, 86400, Malaysia, akhairul@uthm.edu.my

Suriani Abu Bakar
Nanotechnology Research Centre, Faculty of Science and Mathematics, Universiti Pendidikan Sultan Idris, 35900 Tanjung Malim, Malaysia, suriani@fsmt.upsi.edu.my

See next page for additional authors

How to Cite this Article

Mustakim, Nurul Syafiqah Mohamed; Kamaruzaman, Dayana; Parimon, Norfarariyanti; Ahmad, Mohd Khairul; Bakar, Suriani Abu; and Mamat, Mohamad Hafiz (2026) "Hematite/NiO/Graphene Composites: Enhancing Humidity Energy Harvesting Through Temperature Variations," *Baghdad Science Journal*: Vol. 23: Iss. 1, Article 8.
DOI: https://doi.org/10.21123/2411-7986.5134

Hematite/NiO/Graphene Composites: Enhancing Humidity Energy Harvesting Through Temperature Variations

Authors

Nurul Syafiqah Mohamed Mustakim, Dayana Kamaruzaman, Norfarariyanti Parimon, Mohd Khairul Ahmad, Suriani Abu Bakar, and Mohamad Hafiz Mamat

BAGHDAD SCIENCE JOURNAL 2026;23(1):95–107

Scan the QR to view the full-text article on the journal website

SPECIAL ISSUE ARTICLE

Hematite/NiO/Graphene Composites: Enhancing Humidity Energy Harvesting Through Temperature Variations

Nurul Syafiqah Mohamed Mustakim [1], Dayana Kamaruzaman [2], Norfarariyanti Parimon [3], Mohd Khairul Ahmad [4], Suriani Abu Bakar [5], Mohamad Hafiz Mamat [1,*]

[1] NANO-ElecTronic Centre (NET), Faculty of Electrical Engineering, Universiti Teknologi MARA, 40450 Shah Alam, Selangor, Malaysia
[2] Faculty of Electrical Engineering, Universiti Teknologi MARA Cawangan Terengganu, Kampus Dungun, 23000 Dungun, Terengganu, Malaysia
[3] Faculty of Engineering, Universiti Malaysia Sabah, 88400 Kota Kinabalu, Sabah, Malaysia
[4] Microelectronic and Nanotechnology–Shamsuddin Research Centre (MiNT-SRC), Faculty of Electrical and Electronic Engineering, Universiti Tun Hussein Onn Malaysia, Batu Pahat Johor, Parit Raja, 86400, Malaysia
[5] Nanotechnology Research Centre, Faculty of Science and Mathematics, Universiti Pendidikan Sultan Idris, 35900 Tanjung Malim, Malaysia

ABSTRACT

Harvesting energy from humidity is a new approach that has emerged as a potential renewable energy source. However, there are drawbacks to current humidity-based energy-harvesting technologies, such as the absence of a long-term conversion mechanism in hygroscopic materials. In this study, we developed hematite/nickel oxide/graphene (hematite/NiO/Gr) on a cellulose-based substrate as the hygroscopic material for humidity-to-energy applications. We successfully synthesized a novel hematite/NiO/Gr composite using a cost-effective sonicated solution immersion method at different synthesis temperatures. Results indicated that the prepared hygroscopic material is hydrophilic, with a water contact angle of 67.83°. The fabricated humidity-to-energy device utilizing these hygroscopic materials yielded an output voltage of 3.87 ± 0.06 mV and a current density of 0.309 ± 0.05 nA/cm^2. This research highlights the potential of cellulose-based hematite/NiO/Gr composites as promising hygroscopic materials that could be utilized in future large-scale green energy technologies.

Keywords: Cellulose-based, Hematite/NiO/Graphene composite, Hygroscopic, Humidity-to-energy, Renewable energy

Introduction

Harvesting energy from humidity is a viable renewable energy strategy and could serve as a significant source of power that supports other mature technologies such as solar cells,[1,2] nanogenerators,[3,4] and biofuels.[5,6] This technology has been reported as early as 2013,[7] and the development is still ongoing until up to now. Hygroscopic material and working electrodes are the two key components for this technology. Basically, it operates on the principle of hydration-induced ionization effects. Water molecules are absorbed by hygroscopic materials when they are exposed to ambient humidity, resulting in subsequent hydration and the ionization effect, which produces free charge carriers.[8] The hygroscopic materials' gradient structure causes charge carriers to diffuse, generating an electric potential

Received 21 February 2025; revised 12 May 2025; accepted 22 July 2025.
Available online 1 January 2026

* Corresponding author.
E-mail addresses: nurulsyafiqah273@gmail.com (N. S. M. Mustakim), dayana620@uitm.edu.my (D. Kamaruzaman), fara2012@ums.edu.my (N. Parimon), akhairul@uthm.edu.my (M. K. Ahmad), suriani@fsmt.upsi.edu.my (S. A. Bakar), mhmamat@uitm.edu.my (M. H. Mamat).

https://doi.org/10.21123/2411-7986.5134

between the electrodes and initiating a current flow. However, the power output of the current humidity-to-energy conversion based on existing hygroscopic materials is limited by the absence of a sustained conversion mechanism.[9–11] A sustained conversion mechanism is essential in humidity energy harvesting to ensure that the system can continuously convert moisture into electrical energy. Furthermore, most reported humidity-to-energy studies face challenges in scaling up this technology due to the use of costly materials and complex device structures. To develop hygroscopic materials, many studies have relied on intricate synthesis procedures, which limit the scalability of the production process.[12]

These challenges can be resolved by taking into consideration a synthesis process optimization that will influence material modification, particularly in terms of enhancing the material's surface qualities. Reports indicate that ideal synthesis temperatures are crucial for material development, which impacts the overall effectiveness of particular applications. Numerous studies using a range of methodologies on the impact of synthesis temperature variations in various applications are included in Table 1. Optimizing the synthesis temperature can be a strategy in solution to control the surface properties of the developed hygroscopic materials, thereby improving the conversion of humidity to energy.

Table 1. Several studies have been conducted on the effect of synthesis temperature variations for a wide range of applications using various methods.

Material	Application	Method	Synthesis temperature (°C)	Result	Ref.
Carbon dots	Electrode materials	Hydrothermal	180, 220, and 260	• As the temperature of the hydrothermal treatment rises, the size stays constant. • High hydrothermal treatment temperature = higher quantum yields up to 18.1%.	13
Polysaccharide Microgels	Biosensing, controlled drug delivery, and release	Hot water bath	0.6–18.1	• Microgels that deswell at low ΔT are larger, more polydisperse, and have a lower density. • Nonuniform microgels with a low density and a high degree of polydispersity form at high ΔT.	14
Magnetite nanoparticles	Biomedical	Coprecipitation	40, 50, and 60	• Effects the material conductivity and current readings. • At 40 °C = 10^{-6} Ω/m conductivity. • At 50 °C and 60 °C = 10^{-4} Ω/m conductivities.	15
TiO_2 nanorods	Batteries	Hydrothermal	140–180	• 140 °C = higher current rates of 500–1000 mAg^{-1}. • The ideal temperature for mild capacity anode materials with good cycling stability is 160 °C.	16
$CaAl_2O_4$: Eu^{2+}, Dy^{3+}	Lighting devices	Facile solution combustion	300, 400, 500, 600, 700, 800, 900, and 1000	• As the temperature of synthesis increased, the major XRD peaks shifted to higher two theta. • Increase in particle sizes and lattice parameters.	17
Hydroxyapatite	Biomedical	Hydrothermal	98 °C, 110 °C and 120 °C	• The impedance value increased to 1.0×10^5 Ω·cm^2.	18
AgNPs	Microscopic kinetics	Wet chemical	70, 75, 80, 85, and 90.	• Effects the size of nanoparticles under sufficient and insufficient Ag+ precursors.	19
Hydroxyapatite	Biomaterial	Hydrothermal	200 and 230	• HA-230 showed superior results with a lower Ca/P ratio of 2.29, in comparison to HA-200, which had a Ca/P ratio of 2.44. • HA-200 showed an additional XRD peak that correlated with $Ca(OH)_2$ impurities.	20
g-C_3N_4 nanoparticle	Solar energy conversion	Facile one-step molten salt route	450, 500, 550, and 600	• Effects the phase and morphology of g-C_3N_4.	21

According to reports, metal oxides and graphene are significant materials that facilitate charge extraction and stability enhancement because of their energy band-level compatible qualities, cost-effectiveness, and environmental friendliness.[22,23] A highly conductive medium for ion transport is offered by graphene. On the other hand, metal oxide, more especially, nickel oxide (NiO), is a redox transition metal active material with excellent thermal and chemical stability as well as a high theoretical specific capacity, low cost, abundance, and environmental friendliness. Due to their exceptional qualities, graphene and NiO compositions have found widespread use in energy storage devices like batteries and supercapacitors,[23,24] as well as photovoltaic cells.[22] Most studies showed that these composites performed the best electrochemically.[23–25] Another potential metal oxide, iron oxide (Fe_2O_3), which is also known as hematite, is regarded as one of the most significant species of nanomaterials because of its optical, magnetic, electrical, and low-cost characteristics.[26] Numerous applications have made use of it, such as lithium batteries,[27,28] supercapacitors,[29,30] corrosion protection coatings,[31] and photovoltaic cells.[32] The incorporation of hematite can enhance the reaction rates on surfaces by expanding the active interface region,[32] which may improve the material's capacity to absorb moisture and produce charge from ambient humidity. Furthermore, hematite integration can also prevent electron-hole recombination.[32] The efficiency of transforming humidity-induced changes into usable electrical energy can be increased by preserving the generated charges through decreased electron-hole pair recombination.

This study addressed the challenges in scaling up this technology by developing a novel hygroscopic material based on hematite/NiO/Graphene (hematite/NiO/Gr) composites using a cost-effective and straightforward sonication solution immersion method. During the synthesis process, surface modification with varying synthesis temperatures is used to examine the effectiveness of the developed hygroscopic material. For the device configuration, a cellulose-based substrate was used to assess the device performance with respect to humidity response. In conjunction with appropriate scaled-up technology, this study supports future approaches to sustainable energy solutions.

Materials and methods

Materials

Nickel nitrate hexahydrate (Ni $(NO_3)_2{\cdot}6H_2O$) (Sigma-Aldrich), graphene nanoplatelets (99.98%, Techinstro), iron (III) nitrate nonahydrate ($Fe(NO_3)_3{\cdot}9H_2O$) (ACS reagent, ≥98%, Sigma-Aldrich) and hexa-methylene-tetramine (HMT) ($C_6H_{12}N_4$, 99.0%, Sigma-Aldrich) were used as precursor materials and stabilizers. Commercial Whatman Qualitative Grade 1 filter paper with a diameter of 110 mm was used as a cellulose substrate. Commercial silver (Ag) (Mechanic, MCN-DJ002) conductive paste was used for the working electrode.

Synthesis of hematite/NiO/Gr composites powder

A simple sonicated solution immersion method was employed to develop the hematite/NiO/Gr powder. First, mix 0.2 M of Ni $(NO_3)_2{\cdot}6H_2O$, 0.2 M of HMT, and 1.0 weight percent (wt.%) of graphene nanoplatelets into deionized water (DI water), followed by 1 wt.% of $Fe(NO_3)_3{\cdot}9H_2O$ into the mixture. The solution was sonicated for one hour in a sonication chamber (Hwashin Technology Powersonic 405) and then stirred for another hour at 500 rpm to guarantee complete mixing. A 100 mL Schott bottle (DURAN) was then filled with the homogenous mixture, sealed tightly, and kept in an immersion bath at varying temperatures of 75 ˚C, 85 ˚C, and 95 ˚C for an hour (Memmert). After being immersed, the precipitates that developed were filtered. The materials were dried overnight at 36 ˚C to remove excess water molecules. The dried sample was annealed in a chamber furnace (Protherm) for one hour at 500 ˚C to increase its crystallinity. The samples were then treated with stearic acid to increase their hydrophilicity. Fig. 1 depicts the described procedure.

Fabrication of humidity-to energy device

1 g of prepared hematite/NiO/Gr powder was dissolved in 15 mL of clear glue (Chunbe 6603) to create hematite/NiO/Gr paste with a concentration of 66.7 mg/mL. Next, the hematite/NiO/Gr paste was applied to a prepared 15 mm by 15 mm square of cellulose substrate using the doctor blade technique, creating a uniform thin layer of hygroscopic material. In this study, commercial Whatman Qualitative Grade 1 filter paper, measuring 110 mm in diameter, served as the cellulose substrate. The deposited hygroscopic layer was then allowed to dry for an hour at 90 ˚C on a heating surface before the working electrode, which had a contact size of 5 mm by 5 mm, was applied to the film. As shown in Fig. 2, the working electrode was prepared by applying commercial Ag conductive paste to the hygroscopic layer in accordance with the patterned substrate.

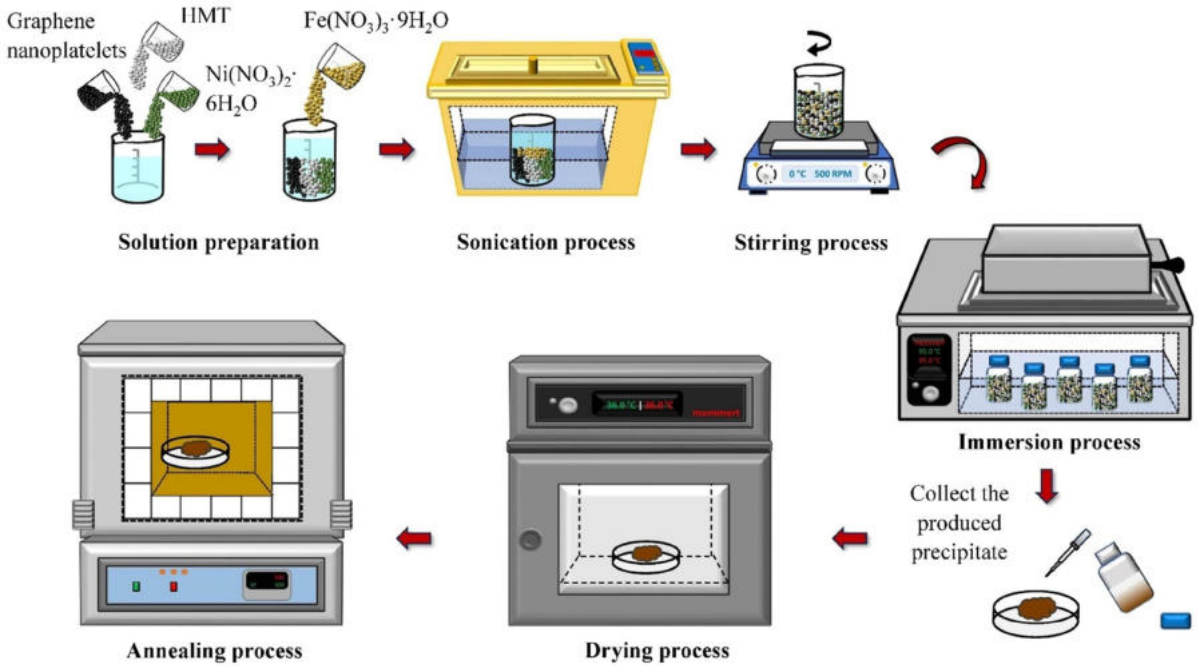

Fig. 1. Synthesis of the hematite/NiO/Gr powder via the sonicated solution immersion method.

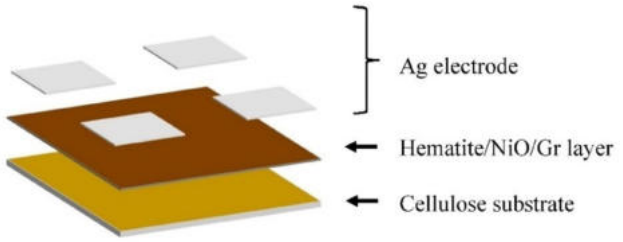

Fig. 2. Device configuration of hematite/NiO/Gr composites layer on cellulose substrate.

Characterizations

Field emission scanning electron microscopy (FE-SEM) (Thermo Scientific, Apreo 2 S; 15 kV of energy operating voltage) integrated with energy dispersive X-ray spectroscopy (EDX; Scanning range of 0 - 10 keV) was used to perform the elemental composition analyses and the morphological investigations for the hematite/NiO/Gr composites. Platinum (Pt) coatings (10 nm thick; auto fine coater, JEOL JFC-1600) were applied to the sample before the EDX measurements to minimize charging in the FESEM images. X-ray diffraction (XRD; Rigaku, UltimaIV) characterization to examine the crystallographic structure and phase development in the 2θ range between 20° and 90° using Cu-Kα1 radiation ($\lambda = 1.5406$ Å). A wafer surface analysis device (VCA-3000, AST product, Inc.) served to measure the water contact angle (WCA) of hematite/NiO/Gr composites on cellulose substrate. A bench-top temperature and humidity chamber (ESPEC-SH261) with a current-voltage-time measuring system (I-V-t; Keithley 2400) was used to perform electrical characterization measurements, specifically to analyze the device's performance and its response to humidity.

Results and discussion

X-ray diffraction analysis

The X-ray diffraction (XRD) patterns of prepared hematite/NiO/Gr powder are shown in Fig. 3. Diffraction peaks at 2θ of 37.3°, 43.44° and 62.96° which corresponds to the (1 1 1), (2 0 0) and (2 2 0)

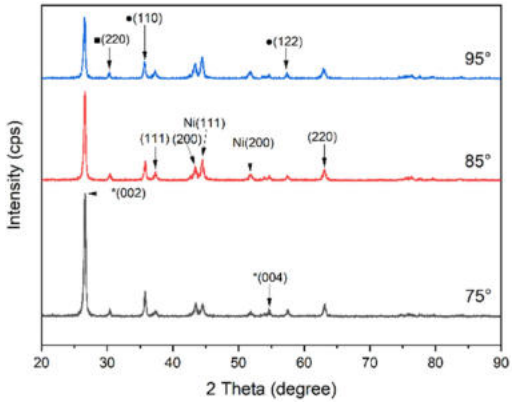

Fig. 3. XRD pattern of hematite/NiO/Gr composites powder at synthesis temperature of 75 °C, 85 °C and 95 °C.

planes, signifying the formation of crystallized cubic NiO nanoparticles (PDF card No. 01-071-4750). The diffraction of pattern at peak 44.44 ° and 51.80° corresponds to the Ni(1 1 1) and Ni(2 0 0), indicating nickel (PDF card No. 004-0850). The XRD patterns clearly exhibit the planes of *(0 0 2) and *(0 0 4) at diffraction peaks 26.52° and 54.66°, respectively, corresponding to crystallized hexagonal graphite (PDF card 56-0160). The diffraction peaks at 35.68° and 57.38° were indexed to the ●(1 1 0) and ●(1 2 2) planes, indicating the formation of crystallized trigonal hematite (PDF card 33-0664). The diffraction peak at 30.42°, which corresponds to the ■(2 2 0), indicates that Fe_3O_4, also known as magnetite (PDF card No. 01-073-9877). This peak arises from the incomplete transformation of iron precursor to hematite.

From XRD results, the crystallite size (D) of hematite, NiO, and graphene nanostructures were calculated from ●(1 1 0), (1 1 1), and *(0 0 2) peak, respectively, by using the Debye–Scherrer Eq. (1):[33]

$$D = \frac{K\lambda}{\beta \cos\theta} \quad (1)$$

Where K stands for a constant, which is set at 0.9, λ is the X-ray wavelength of the XRD ($\lambda = 1.5418$ Å), θ is the diffraction angle, and β is the full width at half maximum (FWHM), which corresponds to the diffraction broadening caused by the crystallite's dimensions.

The estimation of XRD parameters is presented in Table 2. The findings indicate that the synthesis temperature has a significant influence on XRD properties. At a temperature used in synthesis of 75 °C, the crystallite size of hematite particles at the ●(1 1 0) plane is calculated as 23.50 ± 0.78 nm. It slightly increases to 24.29 ± 1.21 nm and 24.42 ± 1.25nm, at higher temperatures of synthesis of 85 °C and 95 °C, respectively. Similarly, the crystallite size of NiO particles at the (1 1 1) plane is estimated to increase from 17.54 ± 2.15 nm to 18.17 ± 1.00 nm as the synthesis temperature rises. These findings align with several reports that have investigated the hematite and NiO structure.[34–37] It is anticipated that higher synthesis temperatures accelerate the reaction rate, resulting in a faster crystallite grain formation process, which, in turn, leads to larger crystallite sizes.[35] Additionally, as observed in the XRD spectra, the intensity of the graphene peak *(0 0 2) decreases from 24.33 ± 0.29 nm to 23.25 ± 0.31 nm with increasing synthesis temperature, consistent with a prior report.[38]

Surface morphological studies

The morphology and microstructure of the synthesized hematite/NiO/Gr composites were examined using FESEM. Fig. 4(a) to 4(c) show the FESEM images of the composites synthesized at different temperatures, while Fig. 4(d) and 4(e) present magnified views of each sample. The images reveal Gr flakes with rippled and layered surfaces, attributed to carbon compression. NiO and hematite particles are randomly dispersed across the Gr flakes, contributing to a porous, electro-conductive structure.[39] The defect sites and edge surfaces of the Gr in the precursor solution act as nucleation centers for the formation of NiO and hematite particles, which subsequently redistribute on the Gr flakes to form heterostructures. The FESEM images also show loosely agglomerated nanoparticles randomly scattered across the surface, with an average diameter ranging from 44 to 97 nm. According to the literature, controlling particle size at the nanoscale is crucial for developing efficient humidity-based energy harvesting devices, as nanoparticles offer higher surface area and enhanced electronic interactions that improve energy conversion and charge transport.[40,41]

As shown in Fig. 4(a), agglomerated nanoparticles are observed at a synthesis temperature of 75 °C, with an average diameter ($Ø_{avg.}$) of 57 ± 7 nm. This suggests that a synthesis temperature of 75 °C furnishes adequate thermal energy to facilitate the nucleation and subsequent crystalline growth of NiO and hematite phases, while simultaneously promoting their effective anchoring and structural integration onto Gr flakes. As the temperature increases to 85 °C, the formation of nanoparticles becomes more pronounced in terms of quantity, accompanied by an increase in particle size, reaching an $Ø_{avg.}$ of approximately 62 ± 10 nm. At 95 °C, the increased formation of nanoparticles results in more extensive

Table 2. The FWHM and crystallite size of hematite ● (1 1 0), NiO (1 1 1), and Gr *(0 0 2) were calculated using the Debye-Scherrer formula.

	●(1 1 0)		(1 1 1)		*(0 0 2)	
Sample	β (rad.)	D (nm)	β (rad.)	D (nm)	β (rad.)	D (nm)
75 °C	$(6.21 \pm 0.21) \times 10^{-3}$	23.50 ± 0.78	$(8.43 \pm 1.03) \times 10^{-3}$	17.54 ± 2.15	$(5.86 \pm 0.07) \times 10^{-3}$	24.33 ± 0.29
85 °C	$(6.01 \pm 0.30) \times 10^{-3}$	24.29 ± 1.21	$(8.35 \pm 0.67) \times 10^{-3}$	17.62 ± 1.39	$(5.90 \pm 0.04) \times 10^{-3}$	24.19 ± 0.16
95 °C	$(5.98 \pm 0.30) \times 10^{-3}$	24.42 ± 1.25	$(8.08 \pm 0.44) \times 10^{-3}$	18.17 ± 1.00	$(6.13 \pm 0.08) \times 10^{-3}$	23.25 ± 0.31

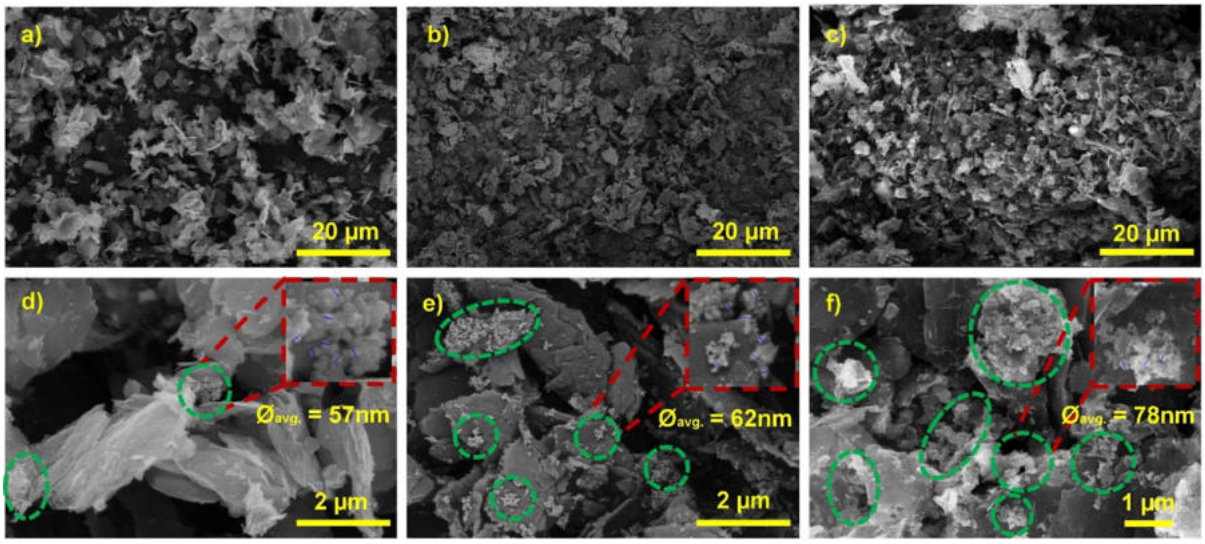

Fig. 4. FE-SEM image of hematite/NiO/Gr composites powder at magnification of 5,000× and 50,000 at synthesis temperature of (a) and (d) 75 °C, (b) and (e) 85 °C, (c) and (f) 95 °C, respectively. The green dashed line indicates regions of nanoparticle agglomeration.

agglomeration, with an $Ø_{avg}$ of 78 ± 13 nm, while still maintaining the nanoscale range. In this study, the maximum synthesis temperature was limited to 95 ˚C due to equipment constraints. These findings demonstrate that the synthesis temperature significantly influences the particles' aggregation behavior. Aggregation occurs due to low electrostatic repulsive barriers, which allow van der Waals attractions to dominate, promoting particle agglomeration.[37,42] Typically, the presence of nanoparticle agglomerates contributes to increased surface roughness and enhances water adsorption.[43–45] However, excessive agglomeration can significantly reduce the effective surface area available for moisture uptake.[46] It is reported that high synthesis temperatures would result in severe nanoparticle aggregation, potentially reducing energy conversion efficiency by restricting moisture diffusion and surface interaction.[47–49] These observations highlight the importance of controlling nanoparticle dispersion to maximize the exposed surface area and enhance water molecule adsorption.

The components of the hematite/NiO/Gr composites were mapped and examined using EDX spectroscopy. The EDX data of the composites, shown in Fig. 5 (a), confirms the presence of the elements carbon (C), nickel (Ni), oxygen (O), and iron (Fe). Peaks appear between 0 and 10 keV. These results are consistent with the XRD spectra, as the EDX spectra show no additional elements. The results are presented in Fig. 5 (a) (inset), indicating that element C signifies the presence of graphene within the composites. The elemental composition and distribution in the composite matrix were further determined by the EDX color mapping shown in Fig. 5 (b) to (g). In this mapping, the colors purple, green, red, and light blue represent elements C, Ni, O, and Fe, respectively. These results confirm the presence and good distribution of all the mentioned elements in the composite matrix.

Water absorption is closely related to hygroscopic materials and hydrophilic properties. It often occurs through the mechanism of chemisorption via noncovalent interactions between hydrophilic functional groups and water molecules.[50] Basically, when exposed to atmospheric moisture, hydrophilic functional groups interact electrostatically or form hydrogen bonds with molecules of water vapor, enabling the hygroscopic material to exhibit water absorption behavior. NiO is known as a strong humidity absorber,[51] while graphene and hematite have been widely used in humidity sensing applications due to their excellent sensing capabilities.[52–54] In this study, hematite/NiO/Gr composites have been utilized as hygroscopic materials with cellulose as the substrate, which enhances water adherence due to the hydrophilic nature of cellulose.

This behavior can be evaluated using the water contact angle (θ_{CA}), which measures the tendency of a liquid to spread on a solid surface. The results in Fig. 6 show that all samples exhibit hydrophilic properties. However, as the synthesis temperature elevates from 75 ˚C to 95 ˚C, the θ_{CA} decreases. This can be attributed to enhanced hydrophilicity resulting from increased surface roughness.[55] As previously discussed, higher nanoparticle agglomeration is evident in the FESEM images as the synthesis temperature rises, leading to greater surface roughness. This results in the creation of more porous spaces,[37,56] which in turn leads to a lower θ_{CA}.

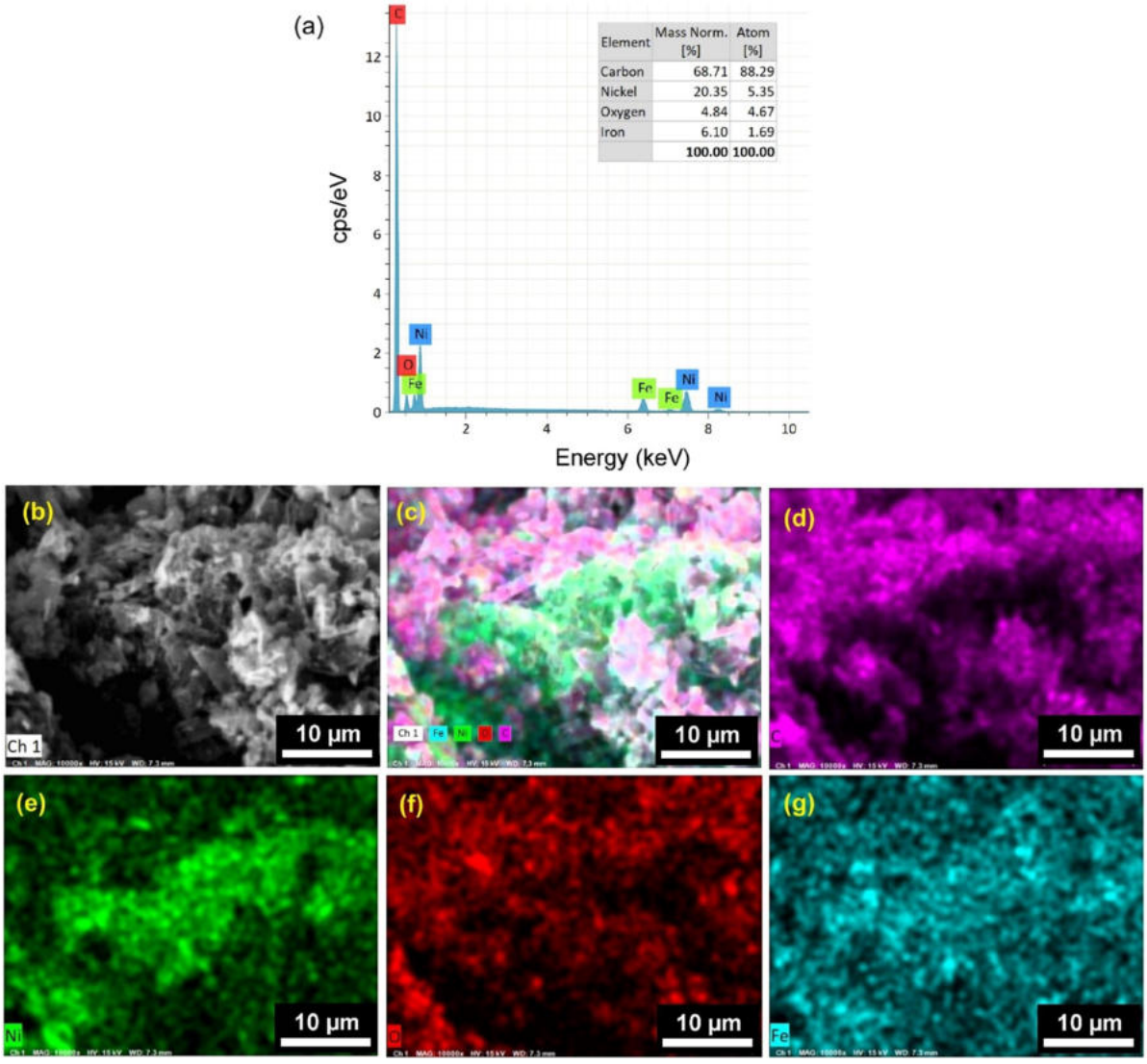

Fig. 5. (a) EDX peaks with analytic elemental composition of hematite/NiO/Gr composites (inset). (b) EDX color mapping: (c) overall mapping, (d) carbon, (e) nickel, (f) oxygen, and (g) iron in the hematite/NiO/Gr composites.

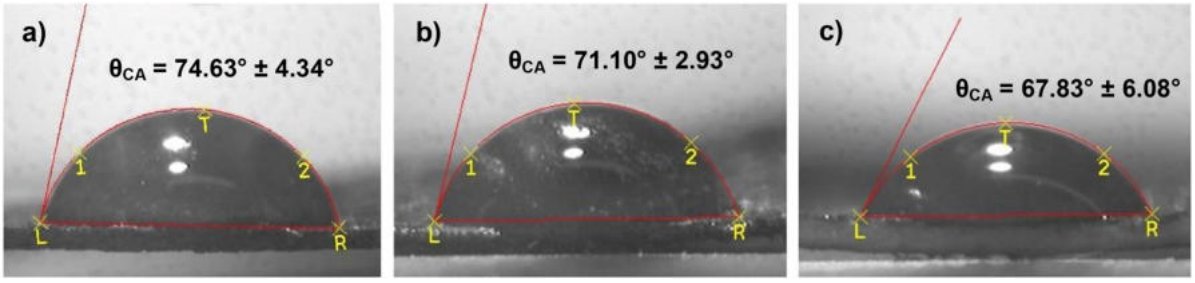

Fig. 6. Water contact angle measurement of hematite/NiO/Gr composites on cellulose-based substrate with different synthesis temperatures (a) 75 °C, (b) 85 °C, and (c) 95 °C.

Humidity response

Measurements were conducted at specific relative humidity (RH) levels to evaluate the samples' response to humidity and their operational effectiveness. Cellulose-based substrates with an area of 1.25 cm^2 were prepared using hematite/NiO/Gr composites synthesized at a range of temperatures, 75 ˚C, 85 ˚C, and 95 ˚C. These were labelled as hematite/NiO/Gr-75, hematite/NiO/Gr-85, and

Table 3. The humidity-to-energy performance of fabricated devices.

Sample	Area, A (cm^2)	RH (%)	Resistance, R (Ω)	Output voltage, V (mV)	Current density, J (nA/cm^2)	Power, P (pW)
Hematite/NiO/Gr-75				3.01 ± 0.23	0.241 ± 0.018	0.91 ± 0.14
Hematite/NiO/Gr-85	1.25	75	10 M	3.45 ± 0.22	0.276 ± 0.018	1.19 ± 0.15
Hematite/NiO/Gr-95				3.87 ± 0.06	0.309 ± 0.005	1.50 ± 0.05

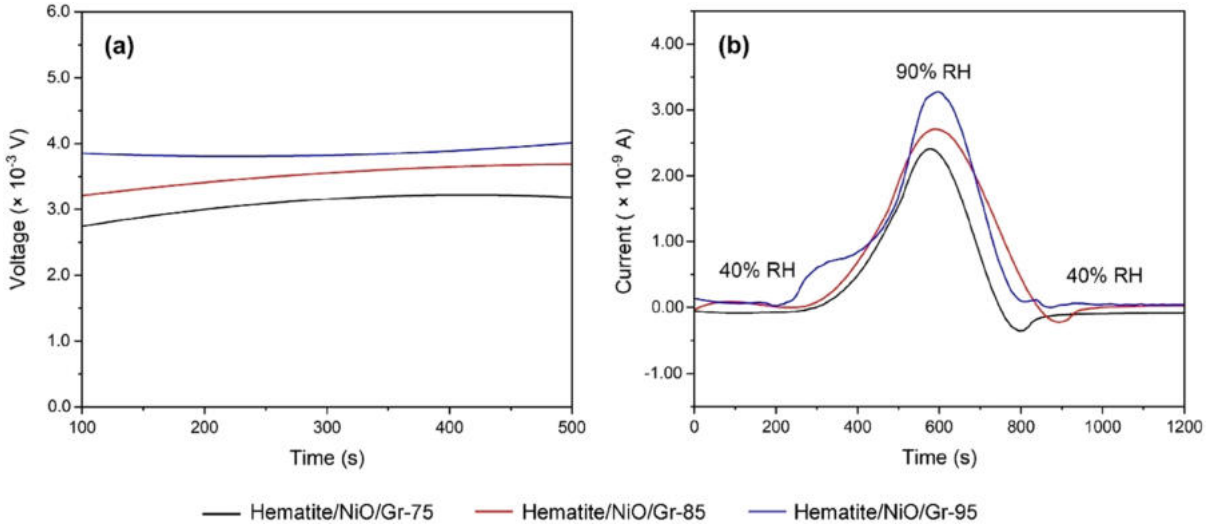

Fig. 7. Response to humidity measurements of hematite/NiO/Gr composites on cellulose-based substrate synthesized at different temperatures (a) The voltage versus time at a fixed RH of 75% with zero bias applied and (b) the current versus time at various RH levels with zero bias applied.

hematite/NiO/Gr-95. The voltage versus time at a fixed RH of 75% is shown in Fig. 7(a), and Table 3 highlights the samples' performance in harvesting humidity into electricity. The results indicate that hematite/NiO/Gr-95 exhibited the best performance, with an output voltage of 3.87 ± 0.06 mV. In comparison, hematite/NiO/Gr-75 and hematite/NiO/Gr-85 generated output voltages of 3.01 ± 0.23 mV and 3.45 ± 0.22 mV, respectively. These findings suggest that synthesis temperature plays a crucial role, as it significantly influences overall power conversion performance. This is primarily due to the hydrophilic properties of each sample, which vary with the synthesis temperature. As discussed earlier, hematite/NiO/Gr-95 exhibits the most enhanced hydrophilic properties compared to hematite/NiO/Gr-75 and hematite/NiO/Gr-85. This allows it to trap more water molecules, thereby producing a notable increase in voltage.[57]

Fig. 7(b) shows the current versus time at varying RH levels. From the graph, all samples demonstrated a good response to humidity changes. They maintained a steady electrical signal at 40% RH and increased steadily as it reached 90% RH during the adsorption process. At 90% RH, hematite/NiO/Gr-95 produced the highest current of 3.28 nA, compared to hematite/NiO/Gr-75 and hematite/NiO/Gr-85, which generated slightly lower currents of 2.41 nA and 2.71 nA, respectively. During the desorption process, as RH decreased from 90% to 40%, all samples showed a drop in current.

Due to the inherent thermal limitations of the experimental setup utilized in this study, the immersion bath temperature was constrained to a maximum of 95 °C, which consequently defined the upper limit of the synthesis conditions investigated. Literature reports, particularly within the scope of humidity-driven energy harvesting applications, underscore that synthesis temperatures exceeding 95 °C can critically modulate nanoparticle physicochemical properties—such as dimensionality, morphological uniformity, and crystallinity—thereby enhancing overall device efficacy.[58,59] However, the optimal synthesis temperature is highly dependent on the material system, synthetic pathway, and targeted functional application.[60–63] For instance, Ni-based metal-organic frameworks (Ni-MOFs) employed in supercapacitor electrodes have shown that materials synthesized at 80 °C exhibit superior specific surface area and enhanced electrochemical response.[64] In contrast, studies on bismuth antimony telluride ($Bi_{0.5}Sb_{1.5}Te_3$) thin films revealed that synthesis

at 150 ˚C yielded powders with maximized thermoelectric and semiconducting performance, thus highlighting the criticality of tailoring synthesis parameters to application-specific requirements.[65]

Conclusion

This research significantly advances the development of materials for humidity-to-energy harvesting by optimizing both material selection and synthesis methods. The study addresses key challenges in achieving stable energy conversion and introduces a novel hygroscopic composite based on hematite/NiO/Gr integrated with cellulose-based substrates. These composites exhibit excellent water absorption and energy conversion capabilities due to their favorable morphological and hydrophilic properties. Fabricated via a cost-effective, low-temperature, sonication-assisted solution immersion technique, the humidity energy harvesting device demonstrated remarkable long-term operational stability, sustaining performance for up to 400 days. Its performance varied with RH level, highlighting its sensitivity and adaptability to environmental changes. Although still in early development, the technology shows strong potential for use in self-powered sensors, wearable electronics, and hybrid energy harvesting systems in humid environments. Crucially, the study affirms that synthesis temperature is a pivotal parameter in modulating key material characteristics to enhance energy harvesting efficiency. Among the evaluated conditions, the composite synthesized at 95 ˚C achieved superior output performance, generating an open-circuit voltage of 3.87 ± 0.06 mV, a current density of 0.309 ± 0.005 nA/cm^2, and a power output of 1.50 ± 0.05pW under 75% RH. Elevated synthesis temperatures facilitated nanoparticle aggregation, increased surface roughness, and enhanced porosity—factors that collectively augmented the material's hydrophilic behavior by lowering the contact angle (θ_{CA}) and improving its humidity responsiveness. Overall, this study underscores the critical role of synthesis temperature in tailoring morphological, hydrophilic, and crystalline properties to maximize the efficacy of humidity-responsive energy conversion systems.

Acknowledgment

The authors express their sincere gratitude to the Ministry of Higher Education Malaysia and the School of Electrical Engineering, College of Engineering, UiTM Shah Alam, for their invaluable support and assistance in facilitating this study. This research project is funded by the Fundamental Research Grant Scheme (FRGS/1/2022/TK07/UITM/02/7). The authors gratefully acknowledge this funding. The generous support from the UiTM Journal Support Fund and Vice Chancellor Special Project (VCSP) (600-RMC/VCSP 5/3 (011/2024)) is sincerely appreciated and gratefully acknowledged.

Authors' declaration

- Conflicts of Interest: None.
- We hereby confirm that all the Figures and Tables in the manuscript are ours. Furthermore, any Figures and images that are not ours have been included with the necessary permission for republication, which is attached to the manuscript.
- No animal studies are present in the manuscript.
- No human studies are present in the manuscript.
- Ethical Clearance: The project was approved by the local ethical committee at Universiti Teknologi MARA, Malaysia.

Authors contributions statement

The authors confirm their contributions to the paper as follows: M.H.M., M.K.A., and S.A.B. designed the study. N.S.M.M., D. K., and N. P. performed the experiment and conducted the data collection. N.S.M.M., M. H. M., N. P., M.K. A., and S. A. B. contributed to the analysis and interpretation of results. N.S.M.M., D.K., and M.H.M. prepared the manuscript draft. All authors approved the final draft of the manuscript after reviewing the findings.

Funding statements

This research project is funded by the Fundamental Research Grant Scheme (FRGS/1/2022/TK07/UITM/02/7). The authors gratefully acknowledge this funding. The generous support of the UiTM Journal Support Fund is sincerely appreciated and gratefully acknowledged.

References

1. Mohamed Mustakim NS, Ubani CA, Sepeai S, Ahmad Ludin N, Mat Teridi MA, Ibrahim MA. Quantum dots processed by SILAR for solar cell applications. Solar Energy. 2018 March 18;163:256–70. https://doi.org/10.1016/j.solener.2018.02.003.
2. Mustakim NS, Sepeai S, Ludin NA, Teridi MAM, Ibrahim MA. Effect of silver sulphide (Ag2S) layer towards the performance of copper indium sulphide (CuInS2) quantum dots sensitised solar cell. International Journal of Nanotechnology.

2020 Jan 1;17(11–12):795–806. https://doi.org/10.1504/IJNT.2020.112383.
3. Kamaruzaman D, Mohamed Mustakim NS, A Subki ASR, Parimon N, Yaakob MK, Malek MF, *et al.* Polystyrene Waste-ZnO nanocomposite film for energy harvesting via hydrophobic triboelectric nanogenerator: Transforming waste into energy. Materials Today Sustainability. 2024 June 1;26:100726. https://doi.org/10.1016/j.mtsust.2024.100726.
4. Mamat MH, Kamaruzaman D, Abdul Aziz A, A Subki ASR, Kamal Ariffin NI, Mohamed Mustakim NS, *et al.* Triboelectric Nanogenerator Based on Tin Doped Zinc Oxide and Polyvinyl Alcohol Composite Thin Film for Energy Harvesting Applications. Journal of Advanced Research in Applied Mechanics. 2024 Oct 30;126(1):165–77. https://doi.org/10.37934/aram.126.1.165177.
5. Malode SJ, Prabhu KK, Mascarenhas RJ, Shetti NP,Aminabhavi TM. Recent advances and viability in biofuel production. Energy Conversion and Management: X. 2021 June 1;10:100070. https://doi.org/10.1016/j.ecmx.2020.100070.
6. Joshiba Ganesan J, Nagarajan D, Rathinam B, Chien J-RC. Low-carbon biofuels from macroalgae towards a sustainable circular bioeconomy and green future. Biomass and Bioenergy. 2024 Nov 1;190:107389. https://doi.org/10.1016/j.biombioe.2024.107389.
7. Ma M, Guo L, Anderson DG, Langer R. Bio-inspired polymer composite actuator and generator driven by water gradients. Science. 2013 Jan 11;339(6116):186–9. https://doi.org/10.1126/science.1230262.
8. Yan H, Liu Z, Qi R. A review of humidity gradient-based power generator: Devices, materials and mechanisms. Nano Energy. 2022 Oct 1;101:107591. https://doi.org/10.1016/j.nanoen.2022.107591.
9. Tianpeng Ding KL, Li J, Xue G, Chen Q, Huang L, Hu B, Zhou AJ. All-printed porous carbon film for electricity generation from evaporation-driven water flow. Adv Funct Mater. 2017 April 3:1700551. https://doi.org/10.1002/adfm.201700551.
10. Daozhi Shen MX, Zou G, Liu L, Duley WW, Norman Zhou Y. Self-powered wearable electronics based on moisture enabled electricity generation. Adv Mater.30(18):e1705925. https://doi.org/10.1002/adma.201705925.
11. Huhu Cheng YH, Zhao F, Yang C, Zhang P, Jiang L, Shi§ G, Qu AL. Spontaneous power source in ambient air of a well-directionally reduced graphene oxide bulk. The Royal Society of Chemistry. 2018 July 17. https://doi.org/10.1039/C8EE01502C.
12. Sun Z, Wen X, Wang L, Ji D, Qin X, Yu J, *et al.* Emerging design principles, materials, and applications for moisture-enabled electric generation. eScience. 2022 Jan;2(1):32–46. https://doi.org/10.1016/j.esci.2021.12.009.
13. Quaid T, Ghalandari V, Reza T. Effect of synthesis process, synthesis temperature, and reaction time on chemical, morphological, and quantum properties of carbon dots derived from loblolly pine. Biomass. 2022 Oct 5;2(4):250. https://doi.org/10.3390/biomass2040017.
14. Freeman KG, Adamczyk J, Streletzky KA. Effect of synthesis temperature on size, structure, and volume phase transition of polysaccharide microgels. Macromolecules. 2020 Oct 21;53(21):9244–53. https://doi.org/10.1021/acs.macromol.0c01605.
15. Gutierrez FV, Lima IS, De Falco A, Ereias BM, Baffa O, Diego de Abreu Lima C, *et al.* The effect of temperature on the synthesis of magnetite nanoparticles by the coprecipitation method. Heliyon. 2024 Feb 29;10(4):e25781. https://doi.org/10.1016/j.heliyon.2024.e25781.
16. Ncube NM, Zheng H. The effect of synthesis temperature on the properties of TiO2 (B) nanorods and its precursors as anode materials for lithium-ion batteries. Materials Research Express. 2020 Jan 6;7(1):015504. https://doi.org/10.1088/2053-1591/ab61bc.
17. NdunguWaithira S, Wako AH, Simba N, Kiprotich S. Effects of synthesis temperature on the sructural and optical propertires of CaAl2O4: Eu2+, Dy3+ Nanoparticles Scientific African. 2024 Oct 18:e02435. https://doi.org/10.1016/j.sciaf.2024.e02435.
18. Wen S, Liu X, Ding J, Liu Y, Lan Z, Zhang Z, *et al.* Hydrothermal synthesis of hydroxyapatite coating on the surface of medical magnesium alloy and its corrosion resistance. Progress in Natural Science: Materials International. 2021 April 1;31(2):324–33. https://doi.org/10.1016/j.pnsc.2020.12.013.
19. Liu H, Zhang H, Wang J, Wei J. Effect of temperature on the size of biosynthesized silver nanoparticle: Deep insight into microscopic kinetics analysis. Arabian Journal of Chemistry. 2020 Jan 1;13(1):1011–9. https://doi.org/10.1016/j.arabjc.2017.09.004.
20. Noviyanti AR, Akbar N, Deawati Y, Ernawati EE, Malik YT, Fauzia RP, *et al.* A novel hydrothermal synthesis of nanohydroxyapatite from eggshell-calcium-oxide precursors. Heliyon. 2020 April 1;6(4):e03655. https://doi.org/10.1016/j.heliyon.2020.e03655.
21. Yang J, Liang Y, Li K, Yang G, Wang K, Xu R, *et al.* One-step synthesis of novel K+ and cyano groups decorated triazine-/heptazine-based g-C3N4 tubular homojunctions for boosting photocatalytic H2 evolution. Applied Catalysis B: Environmental. 2020 March 1;262:118252. https://doi.org/10.1016/j.apcatb.2019.118252.
22. Mahmoudi T, Wang Y, Hahn Y-B. Highly stable perovskite solar cells based on perovskite/NiO-graphene composites and NiO interface with 25.9 mA/cm2 photocurrent density and 20.8% efficiency. Nano Energy. 2021 Jan 1;79:105452. https://doi.org/10.1016/j.nanoen.2020.105452.
23. Agudosi ES, Abdullah EC, Numan A, Mubarak NM, Aid SR, Benages-Vilau R, *et al.* Fabrication of 3D binder-free graphene NiO electrode for highly stable supercapattery. Scientific Reports. 2020 July 8;10(1):11214. https://doi.org/10.1038/s41598-020-68067-2.
24. Singh MK, Krishnan S, Singh K, Rai DK. Effective assembling of nickel oxide-reduced graphene oxide heterostructures for ultrahigh capacity supercapattery. Journal of Power Sources. 2024 March 1;595:234060. https://doi.org/10.1016/j.jpowsour.2024.234060.
25. Kiran A, Hussain S, Ahmad I, Imran M, Saqib M, Parveen B, *et al.* Green synthesis of NiO and NiO@graphene oxide nanomaterials using Elettaria cardamomum leaves: Structural and electrochemical studies. Heliyon. 2024 Oct 30;10(20):e38613. https://doi.org/10.1016/j.heliyon.2024.e38613.
26. Struchalin PG, Thon H, Kuzmenkov DM, Kutsenko KV, Kosinski P, Balakin BV. Solar steam generation enabled by iron oxide nanoparticles: Prototype experiments and theoretical model. International Journal of Heat and Mass Transfer. 2020 Sept 1;158:119987. https://doi.org/10.1016/j.ijheatmasstransfer.2020.119987.
27. Wu Q, Jiang R, Mu L, Xu S. Fe_3O_4 anodes for lithium batteries: Production techniques and general applications. Comptes Rendus Chimie. 2019 Jan 1;22(1):96–102. https://doi.org/10.1016/j.crci.2018.09.016.
28. Zhu W, Kierzek K, Wang S, Li S, Holze R, Chen X. Improved performance in lithium ion battery of CNT-Fe_3O_4@graphene

induced by three-dimensional structured construction. Colloids and Surfaces A: Physicochemical and Engineering Aspects. 2021 March 5;612:126014. https://doi.org/10.1016/j.colsurfa.2020.126014.
29. Feng T, Liu G, Li G, Li Y, Liang J, Wang K. Engineering iron-rich nanomaterials for supercapacitors. Chemical Engineering Journal. 2023 Oct 1;473:145045. https://doi.org/10.1016/j.cej.2023.145045.
30. Kim T, Samuel E, Park C, Aldalbahi A, El-Newehy M, Kang Y, *et al.* Iron oxide supercapacitor of high volumetric energy and power density using binder-free supersonic spraying and self-healing rGO. Ceramics International. 2022 May 15;48(10):13684–94. https://doi.org/10.1016/j.ceramint.2022.01.250.
31. Ayat Monther Alqudsi KAS. Effect of Graphene and Fe_3O_4 on the Protection Efficiency of Polyeugenol Conducted Coating for Stainless Steel 316L in NaCl solution. Baghdad Science Journal. 2024 Nov 1;21(11):3428–37. https://doi.org/10.21123/bsj.2024.8876.
32. Mohamed F, Rabia M, Shaban M. Synthesis and characterization of biogenic iron oxides of different nanomorphologies from pomegranate peels for efficient solar hydrogen production. Journal of Materials Research and Technology. 2020 May 1;9(3):4255–71. https://doi.org/10.1016/j.jmrt.2020.02.052.
33. Huang Y, Cheng H, Yang C, Zhang P, Liao Q, Yao H, *et al.* Interface-mediated hygroelectric generator with an output voltage approaching 1.5 volts. Nature Communications. 2018 Oct 9;9(1):4166. https://doi.org/10.1038/s41467-018-06633-z.
34. Rincón Joya M, Barba Ortega J, Malafatti JOD, Paris EC. Evaluation of Photocatalytic Activity in Water Pollutants and Cytotoxic Response of α-Fe2O3 Nanoparticles. ACS Omega. 2019 Oct 22;4(17):17477–86. http://doi.org/10.1021/acsomega.9b02251.
35. Utari U, Arilasita R, Suharno S, Widiyandari H, Purnama B. Effect of synthesis temperature on structural and magnetic properties in hematite (α-Fe2O3) nanoparticles produced by co-precipitation method. Defect and Diffusion Forum. 2022 Jun 28;417:219–25. https://doi.org/10.4028/p-e8v51k.
36. Taffa DH, Brim E, Rücker KK, Hayes D, Lorenz J, Bisen O, *et al.* Influence of annealing temperature on the OER activity of NiO(111) nanosheets prepared via microwave and solvothermal synthesis approaches. ACS applied materials & interfaces. 2024 Nov 13;16(45):62142–54. https://doi.org/10.1021/acsami.4c14277.
37. Kouhbanani MAJ, Sadeghipour Y, Sarani M, Sefidgar E, Ilkhani S, Amani AM, *et al.* The inhibitory role of synthesized Nickel oxide nanoparticles against Hep-G2, MCF-7, and HT-29 cell lines: the inhibitory role of NiO NPs against Hep-G2, MCF-7, and HT-29 cell lines. Green Chemistry Letters and Reviews. 2021 July 3;14(3):444–54. https://doi.org/10.1080/17518253.2021.1939435.
38. Al-Gaashani R, Zakaria Y, Lee O-S, Ponraj J, Kochkodan V, Atieh M. Effects of preparation temperature on production of graphene oxide by novel chemical processing. Ceramics International. 2021 April 1;47. https://doi.org/10.1016/j.ceramint.2020.12.159.
39. Khaleed AA, Bello A, Dangbegnon JK, Madito MJ, Ugbo FU, Akande AA, *et al.* Gas sensing study of hydrothermal reflux synthesized NiO/graphene foam electrode for CO sensing. Journal of Materials Science. 2017/02/01;52(4):2035–44. https://doi.org/10.1007/s10853-016-0491-6.
40. Zhang J, Boyer C, Zhang YX. Enhancing the Humidity Resistance of Triboelectric Nanogenerators: A Review. Small. 20(36):2401846. https://doi.org/10.1002/smll.202401846.
41. Daripa S, Khawas K, Behere RP, Verma R, Kuila BK. Efficient moisture-induced energy harvesting from water-soluble conjugated block copolymer-functionalized reduced graphene oxide. ACS Omega. 2021/03/23;6(11):7257–65. https://doi.org/10.1021/acsomega.0c03717.
42. Castagnotto E, Locardi F, Slimani S, Peddis D, Gaggero L, Ferretti M. Characterization of the caput mortuum purple hematite pigment and synthesis of a modern analogue. Dyes and Pigments. 2021 Feb 1;185:108881. https://doi.org/10.1016/j.dyepig.2020.108881.
43. Saeed-Ul-Hassan M, Ehtisham M, Badawi AK, Khan AM, Khan RA, Ismail B. A comparative study of moisture adsorption on GO, MOF-5, and GO/MOF-5 composite for applications in atmospheric water harvesting. Nanoscale Advances. 6(14):3668–79. https://doi.org/10.1039/D4NA00150H.
44. Yu H, Mikšík F, Thu K, Miyazaki T. Characterization and optimization of pore structure and water adsorption capacity in pinecone-derived activated carbon by steam activation. Powder Technology. 2024/01/01;431:119084. https://doi.org/10.1016/j.powtec.2023.119084.
45. Gong H, Ma X, Meng S, Wang B, Cui Z. Study on the influence of the agglomeration effect of composite nanoparticles on the photothermal properties of nanofluids. Solar Energy. 2024/03/01/;270:112406. https://doi.org/10.1016/j.solener.2024.112406.
46. Liu X, Gao H, Ward JE, Liu X, Yin B, Fu T, *et al.* Power generation from ambient humidity using protein nanowires. Nature. 578(7796):550–4. https://doi.org/10.1038/s41586-020-2010-9.
47. Hu T, Zhang J, Xia J, Li X, Tao P, Deng T. A review on recent progress in preparation of medium-temperature solar-thermal nanofluids with stable dispersion. Nanomaterials (Basel). Apr 18;13(8). https://doi.org/10.3390/nano13081399.
48. Ma Y, Heil C, Nagy G, Heller WT, An Y, Jayaraman A, *et al.* Synergistic role of temperature and salinity in aggregation of nonionic surfactant-coated silica nanoparticles. Langmuir. 2023/04/25;39(16):5917–28. https://doi.org/10.1021/acs.langmuir.3c00432.
49. Chen X, Wang L, Gao Y, Li Y, Zhang X, Jiang Y, *et al.* Co/N co-doped flower-like carbon-based phase change materials toward solar energy harvesting. Aggregate.5(1):e413. https://doi.org/10.1002/agt2.413.
50. Deng F, Chen Z, Wang C, Xiang C, Poredoš P,Wang R. Hygroscopic Porous Polymer for Sorption-Based Atmospheric Water Harvesting. Advanced Science. 2022 Oct 1;9(33):2204724. https://doi.org/10.1002/advs.202204724.
51. Yang M, Lu J, Wang X, Zhang H, Chen F, Sun J, *et al.* Acetone sensors with high stability to humidity changes based on Ru-doped NiO flower-like microspheres. Sensors and Actuators B: Chemical. 2020 Jun 15;313:127965. https://doi.org/10.1016/j.snb.2020.127965.
52. Zhu C, Tao L-Q, Wang Y, Zheng K, Yu J, L X, *et al.* Graphene oxide humidity sensor with laser-induced graphene porous electrodes. Sensors and Actuators B: Chemical. 2020 Dec 15;325:128790. https://doi.org/10.1016/j.snb.2020.128790.
53. Ahmad WRW, Mamat MH, Zoolfakar AS, Khusaimi Z. The Effect of Ultrasonic Irradiation to Hematite Nanorod Arrays Properties for Humidity Sensor Applications. 19th IEEE International Colloquium on Signal Processing & Its Applications (CSPA). 2023 March 3:144–9. https://doi.org/10.1109/CSPA57446.2023.10087704.
54. Khan MU, Hassan G, Awais M, Bae J. All printed full range humidity sensor based on Fe2O3. Sensors and Actuators A: Physical. 2020 Aug 15;311:112072. https://doi.org/10.1016/j.sna.2020.112072.

55. Cheng Y, Wang M, Sun J, Liu M, Du B, Liu Y, *et al.* Rapid and persistent suction condensation on hydrophilic surfaces for high-efficiency water collection. Nano Letters. 2021 Sept 8;21(17):7411–8. https://doi.org/10.1021/acs.nanolett.1c01928.
56. Zhang P, Zhongnan B, Hongyao Y, Wang R, Guangbao S, Shaoming Z. Effect of particle surface roughness on the flowability and spreadability of Haynes 230 powder during laser powder bed fusion process. Journal of Materials Research and Technology. 2023 Sept 1;26:4444–54. https://doi.org/10.1016/j.jmrt.2023.08.173.
57. Li X, Guo Y, Meng J, Li X, Li M, Gao D. Self-powered carbon ink/filter paper flexible humidity sensor based on moisture-induced voltage generation. Langmuir. 2022 Jun 27;38(27):8232–40. https://doi.org/10.1021/acs.langmuir.2c00566.
58. Kumar S, Thakur VN, Ravikant, Kurchania R, Katiyar RS, Kumar A. Improved humidity sensitivity and possible energy harvesters in lithium modified potassium niobium tantalate oxide. Materials Chemistry and Physics. 2022/09/01/;288:126384. https://doi.org/10.1016/j.matchemphys.2022.126384.
59. Ou C, Sanchez-Jimenez PE, Datta A, Boughey FL, Whiter RA, Sahonta S-L, *et al.* Template-Assisted Hydrothermal Growth of Aligned Zinc Oxide Nanowires for Piezoelectric Energy Harvesting Applications. ACS Applied Materials & Interfaces. 2016/06/08;8(22):13678–83. https://doi.org/10.1021/acsami.6b04041.
60. Anang FEB, Refino AD, Harm G, Li D, Xu J, Cain M, *et al.* Thermo-convective solution growth of vertically aligned zinc oxide nanowire arrays for piezoelectric energy harvesting. Micromachines. 15(10):1179. https://doi.org/10.3390/mi15101179.
61. Duan P, Wang C, Huang Y, Fu C, Lu X, Zhang Y, *et al.* Moisture-based green energy harvesting over 600 hours via photocatalysis-enhanced hydrovoltaic effect. Nature Communications. 2025/01/02;16(1):239. https://doi.org/10.1038/s41467-024-55516-z.
62. Khan M, Salman M, Ullah A, Ullah N, Syed A, Bahkali AH, *et al.* Effect of hydrothermal reaction temperature on MoO3 nanostructure properties for enhanced electrochemical performance as an electrode material in supercapacitors. Ceramics International. 2024/10/01/;50(19, Part A):34943–55. https://doi.org/10.1016/j.ceramint.2024.06.303.
63. Zeng L, Zhang G, Huang X, Wang H, Zhou T, Xie H. Tuning crystal structure of MnO2 during different hydrothermal synthesis temperature and its electrochemical performance as cathode material for zinc ion battery. Vacuum. 2021/10/01/;192:110398. https://doi.org/10.1016/j.vacuum.2021.110398.
64. Shen W, Guo X, Pang H. Effect of Solvothermal Temperature on Morphology and Supercapacitor Performance of Ni-MOF. Molecules.27(23):8226. https://doi.org/10.3390/molecules27238226.
65. Mansouri H, Saberi Y, Sajjadi S. Effect of hydrothermal synthesis temperature on the microstructural and thermoelectric characteristics of thermally deposited Bi0.5Sb1.5Te3 Thin Films. Journal of Electronic Materials. 11/21. https://doi.org/10.1007/s11664-021-09332-6.

المركّبات المكوّنة من الهيماتيت/أكسيد النيكل/الغرافين: تعزيز حصاد طاقة الرطوبة من خلال تغيّرات درجة الحرارة

نُرول شفيقة محمد مستاكيم[1]، ديانا كاماروزمان[2]، نورفراريانتي بريمون[3]، محمد خيرول أحمد[4]، سورياني أبو بكر[5]، محمد حفيظ مامات[1]

[1]مركز الإلكترونيات النانوية*(NET)* ، كلية الهندسة الكهربائية، جامعة مارا للتكنولوجيا، 40450 شاه علم، سيلانغور، ماليزيا.
[2]كلية الهندسة الكهربائية، جامعة مارا للتكنولوجيا – فرع ترنغانو، حرم دونغون، 23000 دونغون، ترنغانو، ماليزيا.
[3]كلية الهندسة، جامعة ماليزيا صباح، 88400 كوتا كيناباالو، صباح، ماليزيا.
[4]مركز أبحاث الميكروإلكترونيات والتقنية النانوية – شمش الدين*(MiNT-SRC)* ، كلية الهندسة الكهربائية والإلكترونية، جامعة تون حسين عون ماليزيا، باتو فاهات، جوهور، باريت راجا، 86400، ماليزيا.
[5]مركز أبحاث التقنية النانوية، كلية العلوم والرياضيات، جامعة السلطان إدريس التربوية، 35900 تانجونغ ماليم، ماليزيا.

الخلاصة

يُعَدّ حصادُ الطاقة من الرطوبة نهجًا جديدًا برز بوصفه مصدرًا محتملاً للطاقة المتجدّدة. ومع ذلك، تُعاني التقنياتُ الحالية المعتمدة على الرطوبة في توليد الطاقة من بعض العيوب، مثل غياب آلية تحويل طويلة الأمد في الموادّ الاسترطابية. في هذه الدراسة، قمنا بتطوير مركّبٍ مكوَّن من الهيماتيت/أكسيد النيكل/الغرافين (Hematite/NiO/Gr) على ركيزةٍ أساسها السليلوز، ليُستخدم مادةً استرطابية في تطبيقات تحويل الرطوبة إلى طاقة. وقد نجحنا في تخليق مركّبٍ جديد من الهيماتيت NiO / Gr /باستخدام طريقة غمرٍ بمحلولٍ مُعرَّضٍ للموجات فوق الصوتية منخفضة التكلفة، عند درجات حرارة تركيبٍ مختلفة. أظهرت النتائج أنّ المادة الاسترطابية المُحضَّرة ذات طبيعة محبّة للماء، إذ بلغ زاوية تماسّها المائي 67.83°. كما أنتج الجهاز المصمَّم لتحويل الرطوبة إلى طاقة باستخدام هذه الموادّ الاسترطابية جهدًا كهربائيًّا مقداره 3.87 ± 0.06 ملّي فولت، وكثافة تيّار بلغت 0.309 ± 0.05 نانو أمبير/سم². وتُبرز هذه الدراسة الإمكانات الواعدة للمركّبات القائمة على السليلوز من نوع هيماتيت / NiO /غرافين بوصفها موادّ استرطابية يمكن الاستفادة منها في تقنيات الطاقة الخضراء واسعة النطاق في المستقبل.

الكلمات المفتاحية: قائمة على السليلوز، مركّب هيماتيت/أكسيد النيكل/غرافين، استرطابية، تحويل الرطوبة إلى طاقة، طاقة متجدّدة.